Journal of Inorganic and Organometallic Polymers and Materials, Vol. 17, No. 2, June 2007 (© 2007)
DOI: 10.1007/s10904-007-9125-4

Transamination Reactivity of $Ti(NMe_2)_4$ and $Zr(NMe_2)_4$ with 1,3,4,5,6-Pentamethyl-2-aminoborazine and Aryl Amines. Model Chemistry for the Formation of Metalloborazine Preceramic Polymers and MN/BN (M = Ti, Zr) Ceramic Composites

Maomin Fan,[1] Eileen N. Duesler,[1] Jerzy F. Janik,[1,2] and Robert T. Paine[1,3]

Submitted July 31, 2006; Accepted September 26, 2006

The transamination reactions between $Ti(NMe_2)_4$ and 1,3,4,5,6-pentamethyl-2-aminoborazine, $(Me)_3N_3(Me)_2B_3(NH_2)$, and diphenylamine (Ph_2NH) and between $[Zr(NMe_2)_4]_2$ and 1,3,4,5,6-pentamethyl-2-aminoborazine, aniline ($PhNH_2$) and diphenylamine have been studied and the molecular product species have been isolated, spectroscopically characterized and single crystal X-ray structure analyses completed. The results of these studies have been used to interpret the outcome of reactions of $Ti(NMe_2)_4$ and $Zr(NMe_2)_4$ with borazinylamine preceramic polymers that, upon pyrolysis, produce TiN/BN, ZrN/BN and $ZrH_{0.6}N$/BN composite powders.

KEY WORDS: Titanium amides; zirconium amides; titanium nitride; zirconium nitride; boron nitride composites; X-ray crystallography

1. INTRODUCTION

A large variety of inorganic polymers have been employed as precursor reagents for the formation of binary non-oxide e.g., boride, carbide, nitride and silicide, ceramic compositions [1, 2]. The organic polymer-like processibility of these preceramic polymers makes it possible to obtain the ceramic materials in technologically useful forms including near-net shape bodies, fibers, coatings, xerogels and aerogels [1–6]. In recent years, with the discovery of increasingly complex polymer compositions, it has also become possible to access ternary and quanternary ceramic compositions with near continuous combining ratios. This allows for considerable flexibility in achieving finished ceramic materials with designed performance properties.

Prior work from our group has shown that poly(borazinylamines) are readily formed in solution reactions of appropriate borazine monomers with disilazane reagents [7–18]. Depending upon the specific borazine monomer, the disilazane coupling agent and the polymer processing steps employed, numerous preceramic polymers are obtained with a range of chemical reactivities built into the structures. Generalized structures for so-called three-point (**1**) and two-point (**2**) polymer structures are shown here. In **1**, the borazine monomer rings are coupled via

We dedicate this paper to Professor Christopher W. Allen in recognition of his distinguished career and his accomplishments in inorganic ring and polymer chemistry.

[1] Department of Chemistry, University of New Mexico, Albuquerque, NM, 87131, USA.
[2] Faculty of Fuels and Energy, AGH University of Science and Technology, al. Mickiewicza 30, 30-059, Krakow, Poland.
[3] To whom correspondence should be addressed. E-mail: rtpaine@unm.edu

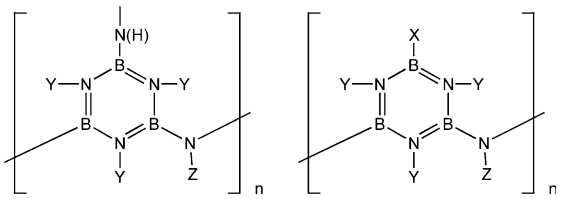

1 2

amino bridge bonds at each boron atom, while in **2** ring coupling occurs through only two of the three boron atoms. The third boron atom carries a terminal group e.g. H, CH_3, $(CH_3)_2N$, NH_2, that does not couple with another ring, but instead introduces a point for reactivity in the polymer. Pyrolysis of the resulting poly(borazinylamines) with X = Y = Z = H or X = NH_2, Y = Z = H, for example, gives good yields of turbostratic (t-BN) or hexagonal (h-BN) boron nitride powders, coatings, fibers, aerogels, aerosols and xerogels [7–18]. Furthermore, the latent reactivity in the B–X bonds in the two-point polymers offer potential for the use of these as reagents for the formation of ternary or composite ceramic compositions.

Traditionally, ceramic composites have been prepared by simple physical blending of micron-sized component particles followed by standard powder processing appropriate for a target finished product. However, as performance demands on finished products have increased, this approach in many examples has proven unsatisfactory. Seeking improved performance, manufacturers attempted to use fine-grain, sub-micron powders and traditional powder blending or newer ball milling methods for the formulation of high performance composites. These methods have provided improvements in product fracture toughness, mechanical strength, thermal shock resistance and microstructure stability. Unfortunately, in many cases, it has proven difficult to routinely obtain and handle pure, crystalline, fine-grained powders and, where available, they often present difficult powder processing obstacles to composite formation. Preceramic polymers and polymer processing methods offer unique strengths for formation of ceramic composites and some recent advances have been reviewed [19].

In the intervening 12 years since that review, interest in nano-scale composite materials has emerged and reactive polymers such as **2** should provide useful entry points where metal functionalization chemistry with B–X, N–Y or N–Z bonds can be achieved. For example, it is well known that homoleptic molecular transition metal amides, $M(NR_2)_x$, containing sterically small R groups, readily undergo transamination/deamination chemistry with formation of new metal amides, imides or mixed amide–imides [20–25]. Pertinent to our study, Bradley and Thomas [26] observed that $Ti(NMe_2)_4$ and $Zr(NMe_2)_4$ (or probably $[Zr(NMe_2)_4]_2$ [27] readily undergo transamination with secondary amines, R_2NH, giving mixed dialkylamides. For example, smaller secondary amines gave $Ti(NMe_2)(NR_2)_3$ (R = Et, Pr, ^{i}Bu) while more bulky examples gave $Ti(NMe_2)_3(NR_2)$ (R = ^{i}Pr, 2,6-dimethylpiperidino (TMP)). Similar products were obtained from $Zr(NMe_2)_4$. Primary amines, RNH_2, with moderately bulky R groups (R = ^{n}Pr, ^{i}Pr, ^{i}Bu, ^{s}Bu, Ph) produced insoluble solids that likely have polymeric structures, $[Ti(NR)]_n$ and $[Zr(NR)(NHR)_2]_n$. With ^{t}BuNH$_2$, dimeric compounds $[(Me_2N)_2Ti(\mu\text{-}N^tBu)]_2$ and $[(Me_2N)_2\ Zr(\mu\text{-}N^tBu)]_2$ have been isolated and structurally characterized by X-ray diffraction [28, 29].

Transamination chemistry has also been employed for the conversion of $Ti(NMe_2)_4$ and $Zr(NMe_2)_4$ to TiN and ZrN by reactions with liquid ammonia [30, 31]. For example, Brown and Maya [30] reported that treatment of $Ti(NMe_2)_4$ and $Zr(NEt_2)_4$ with liquid NH_3 rapidly produced $N(H)Me_2$ and $N(H)Et_2$, respectively and insoluble solids with proposed compositions $Ti_3(NMe_2)_2(NH_2)_2(N)_3$ and $Zr_5(NEt_2)(NH_2)_3(NH)_5(N)_2$ based upon elemental analysis data. Vacuum pyrolyses and thermally programed pyrolyses of the solids revealed formation of $N(H)Me_2$ or $N(H)Et_2$ and NH_3 in the temperature range (200–400°C) and the pyrolysis residues were identified as TiN and ZrN with varying degrees of carbon incorporation depending on pyrolysis conditions. It was suggested that the conversions of the molecular amides and the solid state ammonolysis precursor both involved transamination chemistry by NH_3 as well as deamination of M–NH_2 groups to intermediate imido, M–NH, groups followed by nitride formation. These results have guided numerous chemical vapor deposition (CVD) studies of the $M(NMe_2)_4/NH_3$ systems [32–37].

This observed reaction chemistry suggests that transamination/deamination reactions between $Ti(NMe_2)_4$ and $[Zr(NMe_2)_4]_2$ with a primary amino derivative of **2** (X = NH_2, Y = Z = H) might provide access to metallated preceramic polymers suitable for the formation of TiN/BN and ZrN/BN nano-composites. Preliminary results on this topic were briefly mentioned in our earlier review [19] and additional details on our study are presented here.

2. EXPERIMENTAL

2.1. Materials and Measurements

All manipulations of reagents and reaction products were performed under dry nitrogen atmosphere using standard Schlenk techniques and inert-atmosphere dry boxes. All solvents were rigorously dried and freshly distilled prior to use. Hexamethyldisilazane, aniline and diphenylamine were purchased from Aldrich and distilled prior to use. The samples of 1,3,4,5,6-pentamethyl-2-aminoborazine (**3**) and bis-(1,2,3,4,5-pentamethylborazinyl)amine (**3′**) were prepared as described in the literature [12, 38]. Samples of $Ti(NMe_2)_4$ and $Zr(NMe_2)_4$ were prepared as described in the literature [26, 27]. High purity anhydrous NH_3 was obtained from Matheson Gas Products. Infrared spectra were obtained on a Mattson Galaxy 2020 FT-IR. Mass spectra were recorded on a Finnegan Model 4500 spectrometer using a solids inlet probe enclosed in a dry nitrogen enclosure. NMR spectra were obtained from Bruker AC-250 and JEOL GSX-400 spectrometers using Me_4Si (^1H, ^{13}C) and $F_3B{\bullet}Et_2O$ (^{11}B) as external standards. TGA scans were recorded with a Dupont Model 1090 instrument. Powder X-ray diffraction analyses were obtained with a Scintag PAD-V diffractometer and single crystal X-ray analyses were performed with a Siemens R3m/V automated diffractometer. Elemental analyses were obtained from the UNM Microanalytical Service, Galbraith Laboratories and Pascher Mikroanalytisches Laboratory.

2.2. Synthesis of Molecular Compounds

*2.2.1. (**a**) $\{Me_2N)_2Ti[\mu\text{-}NB_3(Me)_2N_3(Me)_3]\}_2$ (**4**).*

A sample of $Me_3N_3B_3(Me)_2(NH_2)$ (**3**) (0.66 g, 4.0 mmol) in hexane (20 ml) was added (20°C) to a solution of $Ti(NMe_2)_4$ (0.90 g, 4.0 mmol) in hexane (20 ml) and stirred (12 h). During this time, the reaction mixture turned from yellow to red and a red solid formed. Stirring was continued (2d) to ensure complete reaction and then the volatiles were vacuum evaporated. Dimethylamine was identified in the evaporate by FT-IR. The red solid $\{(Me_2N)_2Ti[\mu\text{-}NB_3(Me)_2N_3(Me)_3]\}_2$ **4** was collected by vacuum filtration, washed with cold hexane (3×5 ml) and recrystallized from hot hexane. Yield 0.80 g, 67 %; m.p. 168–170°C . Mass spectrum (30 eV), *m/e* (assignment) inten.: 600 (M^+) 7, 556 ($M - Me_2^+$) 96. Infrared spectrum (KBr, cm^{-1}): 2944 (m), 2903 (m), 2849 (m), 2766 (m), 1607 (w), 1443 (s, br), 1400 (vs, br), 1319 (m), 1279 (m), 1242 (m), 1208 (m), 1184 (m), 1098 (s), 1045 (m), 955 (m), 939 (m), 878 (m), 712 (s), 694 (m), 638 (m), 594 (s). ^1H NMR (C_6D_6): δ 0.59 (B4,6 CH_3, 12H), 2.80 (N5, CH_3, 6H), 3.18 (N(CH_3)$_2$, 24H), 3.35 (N1,3, CH_3, 12H). $^{13}C\{^1H\}$NMR (C_6D_6): δ 0.04 (B4,6, *C*H_3), 34.48 (N5, *C*H_3), 34.96 (N1,3, *C*H_3), 45.10 (N(*C*H_3)$_2$). $^{11}B\{^1H\}$ NMR (C_6D_6): δ −26.0 (*B*2), −36.5 (*B*4,6). Anal. Calcd for $C_{18}H_{54}B_6N_{12}Ti_2$: C, 36.07; H, 9.08; N, 28.04. Found: C, 35.07; H, 9.28; N, 25.90 (small uncombusted residue remained).

*2.2.2. (**b**) $\{(Me_2N)_3\ Zr[\mu\text{-}N(H)B_3(Me)_2N_3(Me)_3]\}_2$ (**5**)*

A sample of **3** (0.74 g, 4.5 mmol) in hexane (20 ml) was added with stirring at 23°C to $Zr(NMe_2)_4$ (1.2 g, 4.5 mmol) in hexane (20 ml). After stirring (1 h), a white precipitate formed. The mixture was additionally stirred (2d) and the solid recovered by vacuum filtration. The volatiles contained Me_2NH as found by IR spectroscopy. The white solid was washed with cold hexane (3×10 ml) and recrystallized from hexane (23°C) leaving colorless single crystals of $\{(Me_2N)_3\ Zr[\mu\text{-}N(H)B_3(Me)_2N_3(Me)_3]\}_2$, **5**. Yield 1.2 g, 69%; m.p. 166–168°C. Mass spectrum (30 eV), *m/e* (assignment) inten.: 315[$(Me)_3N_3B_2(Me)_2BN(H)Zr(NH)NMe_2^+$] 4, 193 [$(Me_2N)_2ZrN^+$] 86, 179 [$(Me_2N)_2Zr^+$]100. Infrared spectrum (KBr, cm^{-1}): 2938 (s), 2911 (s), 2814 (s), 2760 (s), 1605 (s), 1447 (vs), 1383 (vs, br), 1312 (m), 1283 (s), 1240 (m), 1213 (s), 1146 (m), 1099 (s), 945 (m), 928 (s), 883 (m), 733 (m), 718 (s), 615 (m). ^1H NMR (C_6D_6): δ 0.66 (B4, 6 CH_3, 12H), 1.39 (N*H*, 2H), 2.02 ((CH_3)$_2$N, 6H); 2.05 ((CH$_3$)$_2$N, 6H), 2.90 (N5, CH_3, 6H), 2.92 (N(CH_3)$_2$, 24H), 3.21 (N1,3, CH_3, 12H); $^{13}C\{^1H\}$ δ 0.46 (B4, 6 Me), 34.51 (N5 *Me*), 34.90 (N1,3, *Me*), 39.40 (*Me*$_2$N), 43.01 (*Me*$_2$N). $^{11}B\{^1H\}$ NMR (C_6D_6): δ 27.0 (*B*2), 38.0 (*B*4,6). Anal. Calcd for $C_{22}H_{68}B_6N_8Zr_2$: C, 34.04; H, 8.83; N, 25.56. Found: C, 34.28; H, 8.84; N, 24.70.

*2.2.3. (**c**) $[(Me_2N)_5\ Zr_{2.5}(NPh)_3]_2$ (**7**)*

A sample of $PhNH_2$ (0.35 g, 3.7 mmol) in toluene (20 ml) was added to a solution of $Zr(NMe_2)_4$ (1.0 g, 3.7 mmol) in toluene (30 ml) at 0°C. The mixture was stirred at 0°C (3 h) and then at 23°C (12 h). A sample of the volatiles was collected and found by FT-IR to contain Me_2NH. The solution was filtered, the filtrate volume reduced (∼15 ml) and stored for several days at 23°C. Yellow crystals of $[(Me_2N)_5Zr_{2.5}(NPh)_3]_2$ (**7**) deposited. Yield 0.69 g,

63%; decomposes above 100°C. Mass spectrum (30 eV), *m/e* (assignment) inten: 270 [PhNZr $(NMe_2)_2^+$] 7. Infrared spectrum (KBr, cm^{-1}): 2822 (m), 2762 (m), 1582 (s), 1474 (s), 1244 (vs), 936 (m), 885 (m), 756 (s), 694 (m). ^1H NMR (C_6D_6): δ 1.55 (CH_3N, 6H), 1.58 (CH_3N, 6H), 2.65 (CH_3N, 12H), 2.80 (CH_3N, 12H), 3.11 (CH_3N7, 7', 9, 18H) 3.88 (CH_3N9, 6H), 6.50–7.10 (PhN); $^{13}C\{^1H\}$ NMR (C_6D_6): δ 39.29 (CH_3N), 40.58 (CH_3N), 43.24 (CH_3N), 43.55 (CH_3N), 46.62 (CH_3N7, 7', 9), 53.46 (CH_3N9), 117.31, 119.08, 122.27, 124.53, 157.02 (*Ph*N). Anal. Calcd. For $C_{56}H_{90}N_{16}Zr_5$: C, 46.60; H, 6.28; N, 15.52. Found: C, 46.48; H, 6.22; N, 15.16.

2.2.4. (*d*) $(Me_2N)_2$ $Ti(NPh_2)_2$ (*8*)

A sample of Ph_2NH (1.3 g, 7.4 mmol) in toluene (30 ml) was added to $Ti(NMe_2)_4$ (1.7 g, 7.4 mmol) in toluene (20 ml) at 23°C and stirred (2d). The resulting red solution was filtered and the filtrate vacuum evaporated leaving a red oil which was redissolved in hexane and stored at −10°C. Red crystals of $(Me_2N)_2Ti(NPh_2)_2$, **8**, deposited. These were collected and dried under vacuum. Yield: 1.2 g, 67%; m.p. 140–142°C. Mass spectrum (30 eV), *m/e* (assignment) inten: 472 (M^+) 73, 429 ($M - NMe_2^+$) 12, 384 ($M - 2NMe_2^+$) 7, 304 ($M - NPh_2^+$) 100. Infrared spectrum (KBr, cm^{-1}): 3025 (w), 2888 (w), 2859 (w), 2816 (w), 2772 (w), 1931 (w), 1782 (w), 1589 (s), 1481 (vs), 1254 (s), 1177 (s), 934 (s), 870 (s), 750 (s), 694 (s), 505 (m). ^1H NMR (C_7D_8): δ 2.79 (NCH_3, 12H), 6.8–7.2 (N*Ph*). $^{13}C\{^1H\}$ NMR (C_7D_8): δ 44.02 (NCH_3), 122.50 (*Ph*), 122.85 (*Ph*), 129.35 (*Ph*), 151.79 (*Ph*). Anal. Calcd. for $C_{28}H_{32}N_4Ti$: C, 71.18; H, 6.83; N, 11.86. Found: C, 70.84; H, 6.58; N, 11.94.

2.2.5. (*e*) (Me_2N) $Zr(NPh)_3$ (*9*)

A sample of Ph_2NH (1.3 g, 7.5 mmol) in hexane (20 ml) was added with stirring (23°C) to a solution of $(Me_2N)_4Zr$ (1.0 g, 3.8 mmol) in hexane (20 ml). The mixture was stirred (1d) and then refluxed (1d). The volatiles were removed by vacuum evaporation leaving a yellow solid $(Me_2N)Zr(NPh_2)_3$ **9**. The solid was recrystallized from cold hexane. Yield 1.2 g., 75%; m.p. 154–156°C. Mass spectrum (30 eV) *m/e* (assignment) inten.: 640[M^+]13, 639 [M-1^+] 13, 638 [M-2^+] 3, 470 [M–NPh_2–1^+] 100. Infrared spectrum (KBr, cm^{-1}): 2864 (w), 2776 (w), 1483 (vs), 1422 (w), 1312 (w), 1262 (vs), 1181 (s), 1144 (m), 1026 (m), 926 (s), 868 (s), 748 (s), 694 (s). ^1H NMR (C_7D_8): δ 2.19 (NCH_3, 6H), 6.84–7.14 (*Ph*N, 30H); $^{13}C\{^1H\}$ NMR (C_7D_8): 41.13 (CH_3N), 122.72, 123.05, 130.05, 149.34 (*Ph*N). Anal. Calcd for $C_{38}H_{36}N_4Zr$: C, 71.32; H, 5.67; N, 8.75. Found: C, 70.46; H, 5.45; N, 8.90.

2.3. Synthesis of Ceramic Composites

2.3.1. (*a*) Borazinylamine polymers (*11* and *12*)

A sample of the monomer $(Me_2N)B(Cl)_2B_2N_3H_3$ (**10**) [7] (9.93 g, 51.6 mmol) in hexane (100 ml) was combined with hexamethyldisilazane, $(Me_3Si)_2NH$, (8.33 g, 51.6 mmol) and stirred (23°C, 12 h). A white solid formed that was recovered by filtration, washed with hexane (2 × 50 ml) and dried under vacuum. Yield 7.0 g, 98% based upon formation of a polymer with composition $[(Me_2N)B(NHB)_2N_3H_3]_n$ (**11**). Anal. Calcd for $C_2H_{10}N_5B_3$: C, 17.58; H, 7.38; N, 51.25. Found: C, 18.0; H, 7.6, N, 49.9. Infrared spectrum (KBr, cm^{-1}): 3453 (w), 2976 (w), 2953 (w), 2874 (w), 2799 (w), 1524 (vs), 1429 (vs), 1398 (bv, vs), 1250 (m), 1107 (m), 978 (w), 839 (w), 716 (m), 629 (w). This polymeric reagent (7.0 g) was treated with anhydrous $NH_{3(l)}$ (60 ml) (−78°C) and the NH_3 allowed to slowly evaporate (10 h) through a Hg bubbler. The remaining white solid, 5.44 g, corresponds to the polymer $[(NH_2)B(NHB)_2N_3H_3]_n$ (**12**). Anal. Calcd for $B_3N_5H_6$: C, 0.0, H, 5.57; N, 64.49. Found: C, 0.5; H, 6.1; N, 63.8. Infrared spectrum (KBr cm^{-1}): 3486 (m), 3418 (s), 2955 (w), 1607 (s), 1481 (vs), 1375 (br, vs), 1196 (s), 1140 (s), 980 (w), 841 (w), 713 (s), 654 (m).

2.3.2. (*b*) Reaction of poly(borazinylamine) (*12*) with $Ti(NMe_2)_4$

A sample of $Ti(NMe_2)_4$ (5.12 g, 22.8 mmol) in toluene (80 ml) was added to a sample of polymer **12** (2.8 g, ~23 mmol pendant NH_2 groups) in toluene (50 ml). The mixture was stirred (23°C, 2d) then refluxed (2d). Volatiles were vacuum evaporated leaving a black solid (**13**) that was washed with hexane (2 × 50 ml) and vacuum dried. Yield: 4.8 g. The trapped volatiles showed the presence of Me_2NH based upon IR and NMR analysis. The solid was then treated with dry $NH_{3(l)}$ (80 ml) and allowed to stand at 23°C (6 h) while the excess NH_3 slowly boiled off through a Hg bubbler. A brown solid (**14**) was recovered. Yield 3.6 g.

2.3.3. (*c*) Reaction of poly(borazinylamine) (*12*) with $Zr(NMe)_4$

A sample of $Zr(NMe_2)_4$ (6.22 g, 23.3 mmol) in toluene was combined with a sample of polymer **12**

(3.0 g, ~23.4 mmol pendent NH_2 groups) and the mixture treated as described above. The intermediate polymer (**15**) was yellow and it remained yellow following treatment with $NH_{3(l)}$ (**16**). Yield 5.6 g.

*2.3.4. (**d**) Pyrolysis of metallated polymers **14** and **16***

Samples of **14** (0.58 g) and **16** (0.70 g) were placed in boron nitride crucibles and pyrolyzed in a horizontal tube furnace at 1200°C under a slow purge of dry $NH_{3(g)}$. Polymer **14** gave 0.4 g (69%) of a brown solid (**17**). Anal. Found: Ti 43.0; N, 34.4; B, 17.5; C, 0.4, H, 0.1; O, 4.8. Powder XRD (Å): d = 2.446, 2.117, 1.498, 1.277, 1.222. Polymer **16** gave 0.5 g (71%) of a grey solid (**18**). Anal. Found: Zr, 57.3; N, 18.3; B, 9.82; C, 0.10; H, 0.40; O, 14.0. Powder XRD (Å): d = 2.850, 2.642, 2.568, 2.390, 2.282, 1.804, 1.615, 1.548, 1.477, 1.376, 1.320, 1.275, 1.254.

2.4. Crystallographic Measurements for Compounds 4, 5, 7, 8 and 9

Diffraction quality single crystals were obtained from the synthesis work-up procedures described above. Crystals (**4**, 0.16 × 0.18 × 0.35 mm, colorless prism; **5**, 0.09 × 0.25 × 0.30 mm, colorless prism, **7**, 0.21 × 0.34 × 0.55 mm, yellow block; **8**, 0.25 × 0.32 × 0.45 mm, orange-red chip; **9**, 0.16 × 0.32 × 0.51 mm, yellow prism) were mounted in glass capillaries and sealed under dry nitrogen. Data were collected on a Siemens R3m/V diffractometer equipped with a graphite monochrometer and using MoKα radiation (λ = 0.71073 Å). Lattice and data collection parameters are summarized in Table I. Data were collected using variable speed scans at 23°C. All calculations were performed with SHELXTL Plus structure determination programs [39]. Neutral atom scattering factors and anomalous dispersion terms were used for all non-hydrogen atoms during refinements [40]. Full-matrix least-squares methods were utilized in the refinements and the function minimized was $\Sigma w(|F_o|-|F_c|)^2$. The refinements for **4** and **5** were well behaved and all non-hydrogen atoms were refined anisotropically. The H-atoms on the carbon atoms were placed in idealized positions (riding model) and refined with U_{iso} = 1.25 U_{equiv} of the parent atom. The refinement for **7** revealed disorder of the methyl groups on N10: C33, C34 site occupancy 0.61 and C33′, C34′ 0.39. Twofold disorder of the phenyl groups on N1 and N5 was observed and these carbon atoms were refined isotropically. All hydrogen atoms were included for final refinement in idealized positions (riding model for non-disordered carbon atoms and fixed in idealized positions for disordered groups). The refinements for **8** and **9** were well behaved and all non-hydrogen atoms were refined anisotropically. H-atoms were included in idealized positions (riding model) with U_{iso} = 1.25 U_{equiv} of the parent atom.

Table I. Crystallographic Data

	4	**5**	**7**	**8**	**9**
Empirical formula	$C_9H_{27}B_3N_6Ti$	$C_{11}H_{34}B_3N_7Zr$	$C_{56}H_{90}N_{16}Zr_5$	$C_{28}H_{32}N_4Ti$	$C_{38}H_{36}N_4Zr$
Formula weight	299.7	388.1	1443.5	472.5	639.9
Cryst. syst.	Triclinic	Monoclinic	Orthorhombic	Monoclinic	Monoclinic
Space group	$p\bar{1}$	$P2_1/c$	*Pnma*	$P2_1/c$	$C2/c$
a, Å	9.137(2)	22.618(4)	21.425(4)	15.317(3)	21.898(4)
b, Å	9.172(2)	11.008(1)	27.251(5)	11.393(2)	18.940(4)
c, Å	10.990(3)	17.004(2)	11.343(2)	16.758(3)	18.961(4)
α, deg	72.92(2)	90	90	90	90
β, deg	75.81(2)	103.61(1)	90	117.07(3)	124.67(3)
γ, deg	71.90(2)	90	90	90	90
Vol, $Å^3$	824.7(5)	4115(1)	6623(2)	2604.1(8)	6468(2)
Z	2	8	4	4	8
Density, g cm^{-3}	1.207	1.253	1.448	1.205	1.314
μ, mm^{-1}	0.507	0.530	0.807	0.344	0.372
2θ range, deg	2–50	2–47	3–50	3–47	3–52
No. Reflecns. collected	5815	12,661	11,924	7656	13,420
Obs. reflecns.	2258 (F > 3σ(F))	3481 (F > 3σ(F))	3693 (F > 1.5σ(F))	2494 (F > 1.5σ(F))	3292 (F > 2.0σ(F))
R1	0.0475	0.0659	0.0513	0.0443	0.0427
wR2 (all data)	0.0598	0.0610	0.0279	0.0338	0.0341

CCDC reference number 611265 (**5**), 611266 (**4**), 611267 (**8**), 611268 (**7**), 611269 (**9**). Crystallographic data in electronic format may be obtained from the CCDC, 12 Union Road, Cambridge CB2 1EZ, UK or from http://www.ccdc.cam.uc/deposit.

3. RESULTS AND DISCUSSION

3.1. Molecular Model Reactions

In order to better understand and anticipate the reactivity of $Ti(NMe_2)_4$ and $Zr(NMe_2)_4$ with preceramic poly(borazinylamine) reagents, selected model reactions of Group IV metal amides were examined with 1,3,4,5,6-pentamethyl-2-aminoborazine, **3**, and bis-(1,2,3,4,5-pentamethylborazinyl)amine, **3′**. Methyl derivatization of all but one of the borazine ring atoms on **3** and **3′** ensures that its reactivity will solely involve transamination at the *exo* primary amine nitrogen atom (**3**) or the secondary amine nitrogen atom (**3′**). Although not directly related to the preceramic polymer study, reactions of aniline and diphenylamine with $Ti(NMe_2)_4$ and $Zr(NMe_2)_4$ were also explored.

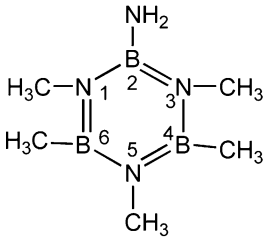

3

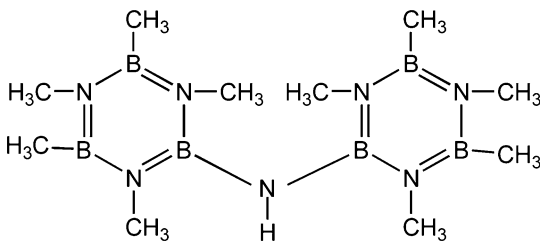

3'

Bradley and Torrible [41] previously observed that reaction of $Ti(NMe_2)_4$ with excess $PhNH_2$ gave a black, relatively insoluble solid that was characterized only by elemental analysis. Based upon those observations, the product was assumed to be a polymeric imido compound $[Ti(NPh)_2]_n$. Bartlett [42] also reported reactions of $PhNH_2$ with $Zr(NMe_2)_4$ in hydrocarbon solvent, and he noted formation of insoluble solids presumed to be Zr(NPh)(NHPh) based upon elemental analysis data. We have reinvestigated these systems and confirm that neat reagent mixtures in hexane and benzene solutions give intractable products. However, as we recently reported when the 1:1 combination of $Ti(NMe_2)_4$ and $PhNH_2$ is performed at 23°C in toluene solution, Me_2NH is released and a red solution is obtained [43]. Upon concentration, red-orange crystals deposit and are recovered in 77% yield. Single crystal X-ray diffraction analysis reveals the formation of an unusual amido–imido Ti bicyclic ring compound, $\{Ti_4(NMe_2)_6(\mu\text{-}NPh)_5]$, **6** [43]. The heavy-atom core structure is shown in Fig. 1. The Ti1 and Ti2 atoms are each bonded to a terminal NMe_2 groups while Ti3 and Ti4 are each bonded to two terminal NMe_2 groups. The N1, N2, N3, N5 and N6 atoms are from bridging PhN–imido groups. All except one nitrogen atom are planar. One NMe_2 group (N4) is slightly distorted (sum of bond angels, 367.8°).

This interesting new observation encouraged additional studies with aniline. We report here that the 1:1 combination of $Zr(NMe_2)_4$ with $PhNH_2$ in toluene held first at 0°C (3 h) and then at 23°C (12 h) produces a yellow solution. Me_2NH is detected by IR analysis of the reaction medium and solution

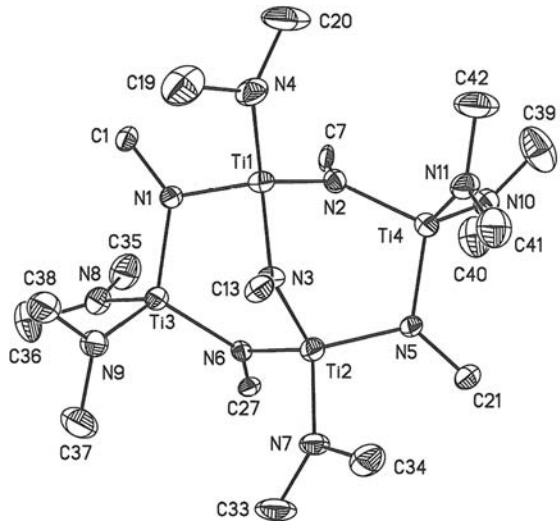

Fig. 1 Heavy atom core structure for $[(Me_2N)_6Ti_4(\mu\text{-}NPh)_5]$, 6 [35].

concentration provides yellow crystals in 63% yield. Single crystal X-ray diffraction analysis shows that this complex is an amido–imido cage compound $[Zr_{2.5}(NMe_2)_5(NPh)_3]_2$, **7**, that is compositionally and structurally distinct from **6**. A view of the full heavy-atom structure is shown in Fig. 2 and a view of the Zr/N atom core structure is shown in Fig. 3. Selected bond lengths and bond angles are presented in Table II. The molecule has a mirror plane that contains N1, N2, N5, N9 and Zr1. There is a central eight-atom cage containing Zr1, Zr2, Zr2′, N1, N2, N5, N7 and N7′, and this cage geometry resembles that adopted in the eight atom core of the compound $[Ti(NMe_2)(N_3)(\mu\text{-}NMe_2)]_3$ $(\mu_3\text{-}N_3)(\mu_3\text{-}NH)$ [44]. In addition, two four-atom *exo* rings containing Zr2, Zr3, N3, N4 and Zr2′Zr3′, N3′, N4′, respectively, are appended to the cage. The Zr1 and Zr2 atoms have distorted trigonal bipyramidal geometries while Zr3 is distorted octahedral. Seven of the dimethyl amido groups have terminal, three coordinate nitrogen

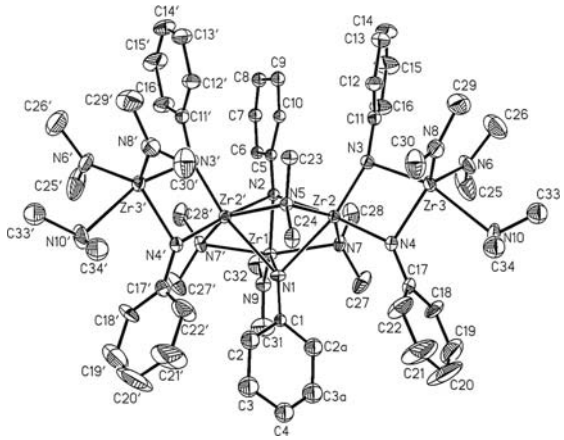

Fig. 2 Molecular structure and atom labeling scheme for $[Zr_{2.5}(NMe_2)_5(NPh)_3]_2$, 7.

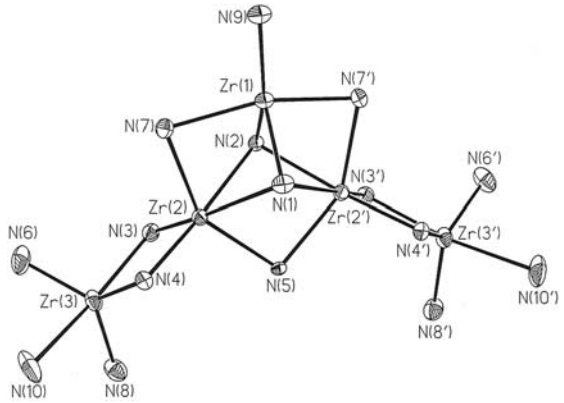

Fig. 3 Heavy atom core structure for $[Zr_{2.5}(NMe_2)_5(NPh)_3]_2$, 7.

Table II. Selected Bond Lengths (Å) and Bond Angles (°) for $[Zr_{2.5}(NMe_2)_5(NPh)_3]_2$, **7**

Bond lengths			
Zr1–N1	2.000(7)	Zr1–N2	2.091(6)
Zr1–N7	2.299(5)	Zr1–N9	2.046(8)
Zr2–N1	2.533(5)	Zr2–N2	2.363(4)
Zr2–N3	1.963(5)	Zr2–N4	2.095(5)
Zr2–N5	2.299(4)	Zr2–N7	2.320(5)
Zr3–N3	2.213(5)	Zr3–N4	2.122(5)
Zr3–N6	2.026(6)	Zr3–N8	2.056(6)
Zr3–N10	2.496(7)	Zr1•••Zr2	3.130(1)
Zr2•••Zr2′	3.401(1)	Zr2•••Zr3	3.192(1)
N1–C1	1.414(11)	N2–C5	1.412(10)
N3–C11	1.413(9)	N4–C17	1.414(9)
N5–C23	1.499(10)	N5–C24	1.481(10)
N6–C25	1.426(10)	N6–C26	1.449(10)
N7–C27	1.482(8)	N7–C-28	1.462(8)
N8–C29	1.429(9)	N8–C30	1.432(10)
N9–C31	1.449(12)	N9–C32	1.442(12)
N10–C33	1.429(16)	N10–C34	1.577(16)
Bond angles			
N1–Zr1–N2	84.0(2)	N2–Zr1–N7	79.6(1)
N1–Zr1–N7	86.5(1)	N1–Zr1–N9	131.5(3)
N2–Zr1–N9	144.5(3)	N7–Zr1–N9	99.9(1)
N7–Zr1–N7′	158.6(2)	N1–Zr2–N3	167.7(2)
N1–Zr2–N2	67.9(2)	N1–Zr2–N4	107.8(2)
N2–Zr2–N3	100.5(2)	N3–Zr2–N4	84.2(2)
N1–Zr2–N5	74.2(2)	N2–Zr2–N5	80.3(2)
N3–Zr2–N5	100.4(2)	N4–Zr2–N5	104.1(2)
N1–Zr2–N7	74.9	N2–Zr2–N7	73.9(2)
N3–Zr2–N7	106.7(2)	N4–Zr2–N7	99.8(2)
N4–Zr3–N6	123.3(2)	N3–Zr3–N4	77.7(2)
N3–Zr3–N8	105.9(2)	N3–Zr3–N6	95.4(2)
N6–Zr3–N8	117.9(2)	N4–Zr3–N8	118.1(2)
N3–Zr3–N10	160.2(2)	N4–Zr3–N10	84.5(2)
N6–Zr3–N10	87.1(2)	N8–Zr3–N10	89.9(2)
Zr2–N1–C1	128.6(3)	Zr1–N1–Zr2′	86.5(2)
Zr2–N1–Zr2′	84.4(2)	Zr1–N2–C5	131.4(5)
Zr1–N2–Zr2	89.1(2)	Zr2–N3–C11	155.0(4)
Zr2–N3–Zr3	99.5(2)	Zr2–N4–Zr3	98.4(2)
Zr2–N2–Zr2′	92.1(2)	Zr3–N4–C17	122.7(4)
Zr2–N3–Zr3	99.5(2)	Zr2–N5–C24	112.7(3)
Zr3–N3–C11	105.5(4)	Zr2–N5–Zr2′	95.4(2)
Zr2–N4–C17	138.8(4)	Zr3–N6–C26	128.0(5)
Zr2–N5–C23	115.5(3)	Zr1–N7–Zr2	85.3(2)
C23–N5–C24	105.3(6)	Zr2–N7–C27	122.3(4)
Zr3–N6–C25	123.1(5)	Zr2–N7–C28	115.9(4)
C25–N6–C26	108.7(6)	C29–N8–C30	110.8(6)
Zr1–N7–C27	111.3(3)	Zr1–N9–C32	124.3(6)
Zr1–N7–C28	113.8(4)	C31–N9–C32	110.6(7)
C27–N7–C28	106.8(5)		
Zr3–N8–C30	124.3(5)		
Zr1–N9–C31	125.0(6)		

atoms: N6, N8, N9, N10, N6′, N8′, N10′. Five of these are planar, N6, N8, N9, N6′, N8′, with an average Zr–N bond length 2.047 ± 0.021 Å (range: 2.026(6) A–2.056(6) Å) while two are pyramidal,

N10, N10′ with Zr–N bond length, 2.50(1) Å. The geometry and bond lengths for the former group are consistent with strong Zr–N dπ–pπ orbital overlaps and these are comparable to structural features in a number of other zirconium amide compounds [45, 46]. The coordination features for N10 and N10′ are consistent with σ-only overlap. The remaining three dimethyl amido groups, N5, N7, N7′, act as four coordinate bridging groups with Zr1–N7 2.299(5) Å, Zr2–N7 2.320(7) Å and Zr2–N5 2.299(4) Å. All six phenyl imido groups act as bridging ligands. Four reside in the two *exo* planar four-membered Zr_2N_2 rings and the N atoms N3, N4, N3′, N4′ are three coordinate and doubly bridging, μ_2. The Zr–N bond lengths in these four-membered rings are asymmetric with the shorter distances associated with the more highly coordinated Zr2(Zr2′): Zr2–N3 1.963(5) Å, Zr2–N4 2.095(5) Å, Zr3–N3 2.213(5) Å, Zr3–N4 2.122(5) Å. The remaining two phenyl imido groups participate in the central cage bonding, and the N atoms, N1 and N2, are four coordinate, triply bridging, μ_3. The Zr–N bond lengths are asymmetric with the shorter distances associated with the distorted trigonal bipyramidal Zr1 atom: Zr1–N1 2.000(7) Å, Zr1–N2 2.091(6) Å. The longer bond lengths involve the distorted octahedral geometry Zr2(Zr2′) atoms: Zr2–N1 2.533(5) Å, Zr2–N2 2.364(4) Å. The non-bonded Zr1•••Zr2 and Zr2•••Zr3 distances, 3.130(1) Å and 3.192(1) Å are slightly longer than observed in the dimeric structure of $[(Me_2N)_2Zr(N^tBu)_2]_2$, 3.092(1) Å [29].

With the molecular structure of **7** known, the elemental analysis for the compound can be interpreted and is in good agreement with the composition deduced in the structure analysis. However, probably as a result of low volatility, a mass spectrum containing an appropriate parent ion was not detected by standard FAB MS techniques. There are six unique NMe_2 groups in the solid-state structure, and six methyl proton resonances are resolved in the ^1H NMR spectrum at δ 1.55, 1.58, 2.65, 2.80, 3.11 and 3.88 and in the $^{13}C\{^1H\}$NMR spectrum, δ 39.29, 40.58, 43.24, 43.55, 46.62 and 53.46.

Given the new results outlined above, the reactions of $Ti(NMe_2)_4$ and $Zr(NMe_2)_4$ with diphenylamine were also explored. The 1:1 combination of $Ti(NMe_4)_4$ and Ph_2NH in toluene solution at 23°C gave a red liquid that crystallized over several days. Elemental analysis is consistent with a formulation $(Me_2N)_2$ $Ti(NPh_2)_2$, **8**, and a FAB MS analysis shows a parent ion at *m/e* 472. The ^1H and $^{13}C\{^1H\}$ NMR spectra show one methyl group and one phenyl group environment, respectively. Single crystal X-ray diffraction analysis was completed for **8**. A view of the molecule is shown in Fig. 4, and selected bond lengths and bond angles are presented in Table III. The compound is monomeric with two terminal, planar NMe_2 groups and two terminal NPh_2 groups bonded to the Ti(IV). The Ti(IV) geometry is tetrahedral with N1–Ti–N2 114.4° and N3–Ti–N4 115.3°. The Ti–NMe_2 bond lengths, Ti–N3 1.859(4) Å and Ti–N4 1.880(3) Å (avg. 1.870 Å) are comparable to the average Ti–NMe_2 bond length in **6**, 1.877(5) Å [43]. The distance in **8** is shorter than the average Ti–N bond length in $(Me_2N)_4Ti$, 1.908(2) Å [47]. However, the Ti–N bond length in **8** is slightly longer than the distance in $(Et_2N)TiCl_3$, 1.852(4) Å [48]. The bond shortening in the latter compound is consistent with increased dπ–pπ overlap with a more electropositive Ti(IV) center due to the presence of the chlorine substituents. The Ti–NPh_2 bond lengths, Ti–N1 1.972(3) Å and Ti–N2 1.962(3) Å (avg. 1.967 Å), are significantly longer than the Ti–NMe_2 bond lengths consistent with weaker dπ–pπ overlap in the Ti–NPh_2 bonds. Several attempts to prepare $(Me_2N)_3Ti(NPh_2)$ and $(Me_2N)Ti(NPh_2)_3$ by using appropriate reactant stoichiometries failed to give pure products and, under the conditions explored, **8** appears to be the favored thermodynamic species.

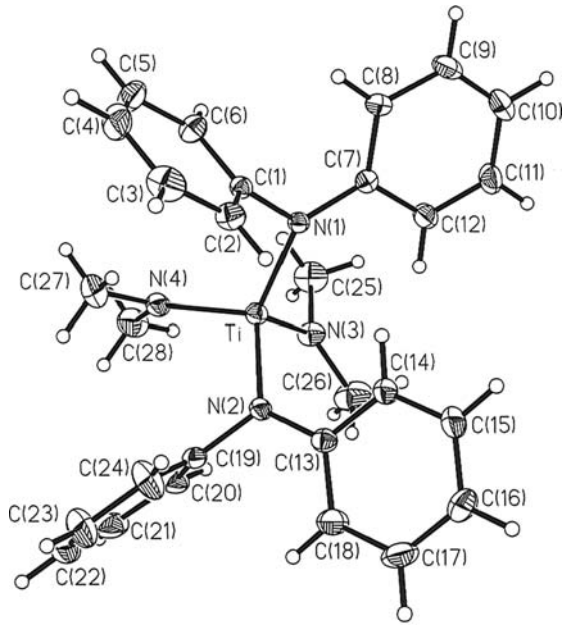

Fig. 4 Molecular structure and atom labeling scheme for $(Me_2N)_2Ti(NPh_2)_2$, 8.

Table III. Selected Bond Lengths (Å) and Bond Angles (°) for $(Me_2N)_2Ti(NPh_2)_2$. **8**

Bond lengths			
Ti–N1	1.972(3)	N1–C1	1.434(5)
Ti–N2	1.962(3)	N1–C7	1.413(4)
Ti–N3	1.859(4)	N2–C13	1.414(5)
Ti–N4	1.880(3)	N2–C19	1.428(4)
N3–C25	1.468(5)	N4–C27	1.452(6)
N3–C26	1.455(5)	N4–C28	1.464(6)
Bond angles			
N1–Ti–N2	114.4(1)	Ti–N1–C1	109.8(2)
N1–Ti–N3	109.5(1)	Ti–N1–C7	132.9(3)
N1–Ti–N4	115.3(1)	C1–N1–C7	116.9(3)
N2–Ti–N4	106.0(1)	Ti–N2–C13	128.1(2)
N2–Ti–N3	104.6(1)	Ti–N2–C19	116.1(2)
N3–Ti–4	106.2(2)	C13–N2–C19	115.6(3)
Ti–N3–C25	115.0(3)	Ti–N4–C27	120.6(3)
Ti–N3–C26	131.0(3)	Ti–N4–C28	127.6(3)
C25–N3–C26	114.0(3)	C27–N4–C28	110.9(3)

The reaction of $Zr(NMe_2)_4$ with Ph_2NH was examined with several reagent combining ratios and solvents. The reaction is more sluggish and gives mixtures of products. The cleanest results were obtained with $Ph_2NH/Zr(NMe_2)_4$ 2:1 in hexane at 23°C (1d) followed by reflux (1d). Yellow crystals, isolated in 75% yield, are found to be $Zr(NMe_2)(NPh_2)_3$, **9**. The compound is analytically pure following recrystallization from hexane and the parent ion is detected by FAB MS. The ^1H and ^{13}C NMR spectra display single methyl group and single phenyl group environments consistent with the proposed formulation.

The molecular structure for **9** was confirmed by single crystal X-ray diffraction analysis. A view of the molecule is shown in Fig. 5 and selected bond lengths and bond angles are given in Table IV. The molecule is monomeric with one terminal, planar NMe_2 group and three terminal, planar NPh_2 groups. The Zr(IV) geometry is tetrahedral with N1–Zr–N2 107.8(2)°, N1–Zr–N4 117.4(2)°, N3–Zr–N4 109.7(2)°, N2–Zr–N3 109.9(2)°. The Zr–NMe_2 bond length, Zr–N4, 2.007(4)Å is shorter than the Zr–NPh_2 bond lengths, Zr–N1 2.071(4) Å, Zr–N2 2.094(3) Å and Zr–N3 2.104(4) Å (avg. 2.090 Å). The latter are actually more similar to the average terminal Zr–NMe_2 bond length in $(Me_2N)_4Zr$, 2.069(3) Å (range 2.045(3)–2.108(3) Å) [27]. The shorter Zr–N4 distance is consistent with stronger Zr–NMe_2 dπ–pπ overlap.

Of more direct relationship to our efforts to obtain MN/BN composites from poly(borazinylamine)/metal amide precursors are reactions between

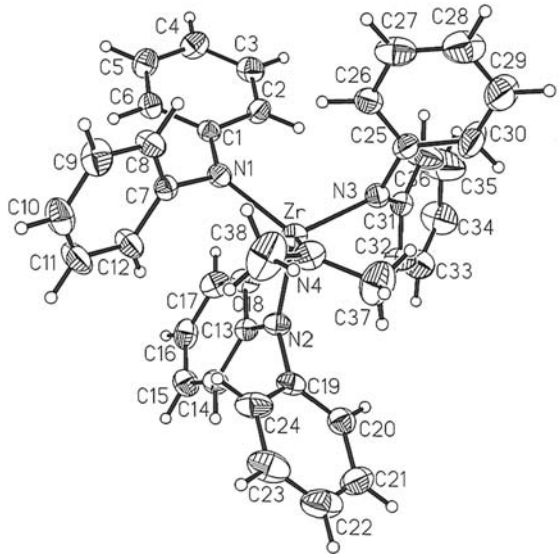

Fig. 5 Molecular structure and atom labeling scheme for $(Me_2N)Zr(NPh_2)_3$, 9.

Table IV. Selected Bond Lengths (Å) and Bond Angles (°) for $(Me_2N)Zr(NPh_2)_3$. **9**

Bond lengths			
Zr–N1	2.071(4)	Zr–N2	2.094(3)
Zr–N3	2.104(4)	Zr–N4	2.007(4)
N1–C1	1.405(5)	N1–C7	1.441(6)
N2–C13	1.403(6)	N2–C19	1.439(5)
N3–C25	1.427(6)	N3–C31	1.411(6)
N4–C37	1.450(9)	N4–C38	1.449(6)
Bond angles			
N1–Zr–N2	107.8(2)	N1–Zr–N3	107.1(1)
N1–Zr–N4	117.4(2)	N3–Zr–N4	109.7(12)
N2–Zr–N3	109.9(1)	N2–Zr–N4	104.8(1)
Zr–N1–C1	136.4(3)	Zr–N1–C7	106.0(3)
C1–N1–C7	117.6(4)	C13–N2–C19	116.0(3)
Zr–N2–C13	123.9(2)	Zr–N2–C19	119.6(3)
Zr–N3–C25	111.5(3)	Zr–N3–C31	131.0(3)
C25–N3–C31	117.1(4)	Zr–N4–C37	113.1(3)
Zr–N4–C38	135.3(4)	C37–N4–C38	111.2(4)

$Ti(NMe_2)_4$ and $Zr(NMe_2)_4$ with **3** and **3′**. The 1:1 reaction of **3** with $Ti(NMe_2)_4$ in hexane at room temperature gives a red solution from which a red solid deposits in 67% yield. Recrystallization provides red crystals, and the identity of the compound was deduced by single crystal X-ray diffraction analysis. The molecule is a dimeric complex, $\{(Me_2N)_2Ti[\mu\text{-}NB_3(Me)_2N_3(Me)_3]\}_2$, **4**. A view of the molecule is shown in Fig. 6 and selected bond angles and distances are summarized in Table V. The structure contains a planar, centrosymmetric Ti_2N_2 ring that is comparable

with the dimeric ring structure displayed by $[(Me_2N)_2Ti(\mu\text{-}N^tBu)]_2$ [28]. The ring bridging imido nitrogen atom originates from the terminal $-NH_2$ group of the borazinylamine **3**. In order to minimize strain, the pentamethyl borazine rings rotate so that they are perpendicular to the Ti_2N_2 plane. Although very similar in structure, the Ti_2N_2 ring in **4** is much more asymmetric than the ring in $[(Me_2N)_2Ti(\mu\text{-}N^tBu)]_2$. This is shown by comparison of the Ti–N(ring) bridge bond lengths in **4**, Ti–N1 1.947(2) Å and Ti–N1 1.913(3) Å with those in $[(Me_2N)_2Ti(\mu\text{-}N^tBu)]_2$, 1.921(2) and 1.925(2) Å. The bridge bond lengths in **4** are also longer than the terminal Ti–NMe_2 bond lengths, Ti–N5 1.919(3) Å and Ti–N6 1.895(3) Å and these compare favorably with the terminal Me_2N–Ti bond lengths in $[(Me_2N)_2Ti(\mu\text{-}^tBu)]_2$, 1.913(2) and 1.914(2) Å [28]. Each amido and imido nitrogen atom (N1, N5, N6) is planar with the largest deviation represented by the bond angle sum on N1, 357.0°. In view of the MO arguments presented by Thorn et al. [28], it appears that the asymmetric Ti_2N_2 ring structure in **4** is very likely driven by electronic differences between the borazine ring and ^{t}Bu group on the bridging imido nitrogen atom.

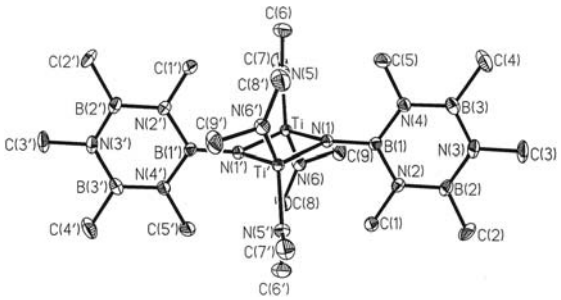

Fig. 6 Molecular structure and atom labeling scheme for $\{(MeN)_2Ti[\mu\text{-}NB_3(Me)_2\ N_3(Me)_3]\}_2$, 4.

Table V. Selected Bond Lengths (Å) and Bond Angles (°) for $\{(Me_2N)_2Ti[\mu\text{-}N\ B_3(Me)_2N_3(Me)_3]\}_2$. **4**

Bond lengths			
Ti–N1	1.947(2)	B1–N1	1.467(5)
Ti–N1′	1.913(3)	B1–N2	1.445(4)
Ti–N5	1.919(3)	B1–N4	1.440(6)
Ti–N6	1.895(3)	B2–N2	1.449(6)
Ti•••Ti′	2.793(1)	B2–N3	1.427(7)
N2–C1	1.459(6)	B3–N3	1.428(5)
		B3–N4	1.435(6)
N3–C3	1.470(6)	B2–C2	1.574(6)
N4–C5	1.478(4)	B3–C4	1.586(8)
N5–C6	1.453(5)	N6–C8	1.446(6)
N5–C7	1.460(5)	N6–C9	1.451(7)
Bond angles			
N1–Ti–N1′	87.3(1)	Ti–N1–Ti′	92.7(1)
N1–Ti–N5	115.7(1)	N1–Ti–N6	112.9(1)
N5–Ti–N6	107.0(1)	N5–Ti–N1′	117.2(1)
N6–Ti–N1′	116.0(1)	Ti–N1–B1	127.0(2)
B1–N1–Ti′	137.3(2)	N1–B1–N2	122.6(4)
C6–N5–C7	109.9(3)	Ti–N5–C6	126.7(2)
Ti–N5–C7	123.4(3)	Ti–N6–C9	112.2(3)
Ti–N6–C8	135.2(3)	C8–N6–C9	112.0(3)

The structure determined for **4** is consistent with its mass spectrum which shows a dimer parent ion, $m/e = 600$. However, the CHN data for the compound are typically low in C and N suggesting that a minor impurity is retained in the analytical samples, or combustion of the sample is incomplete as noted in analysis reports. The ^{1}H NMR spectrum shows single resonances for the methyl groups on the boron atoms (B4, B6, δ 0.04), the methyl groups on the borazine N atoms (N5, δ 2.80; N1,3 δ 3.35) and on the Me_2N groups (δ 3.18). There is no resonance observed for a N*H* proton and this is consistent with the presence of the borazinyl imide. Similarly, the $^{13}C\{^1H\}$ NMR spectrum shows single resonances at δ 0.04 (B4,6), 34.48 (N5*C*H$_3$), 34.96 (N1,3, *C*H$_3$), 45.10 (N*Me*$_2$). The $^{11}B\{^1H\}$ NMR spectrum shows two broad resonances at δ −26.0 (B2) and −36.5 (B4,6) in a 1:2 ratio.

The reaction of $Ti(NMe_2)_4$ and **3** was also examined with a 1:2 reactant stoichiometry and **4** was obtained as a red crystalline solid identified by its mass spectrum and ^{1}H NMR spectrum. Since the poly(borazinylamine) used to obtain preceramic composite oligomers contains fragments such as represented by **17**, reactions of $Ti(NMe_2)_4$ with the ring permethylated compound $(Me_3N_3B_3Me_2)_2NH$, **3′** were also examined with hexane or toluene as solvent. No reaction was noted after two days at room temperature or at reflux. This suggests that transamination reactions of the $Ti(NMe_2)_4$ with the preceramic oligomer **12** should occur only at the *exo* B–NH_2 group.

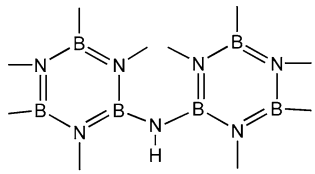

17

The 1:1 reaction of **3** with $Zr(NMe_2)_4$ in hexane at 23°C was also examined. This combination gives a white solid in 69% yield that crystallized as colorless single crystals. The composition and structure of this compound was determined by single crystal X-ray diffraction analysis. The compound, $\{(Me_2N)_3Zr[\mu\text{-}N(H)B_3(Me)_2N_3(Me)_3]\}_2$ **5**, is distinctly different in

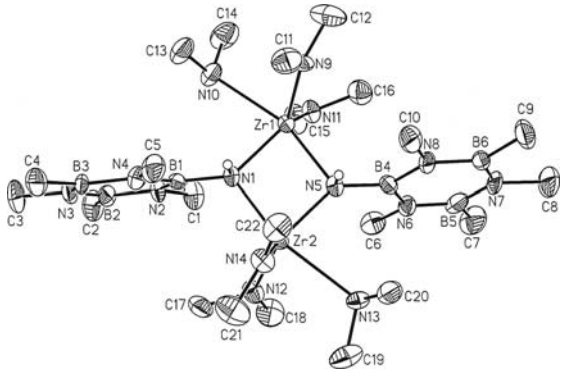

Fig. 7 Molecular structure and atom labeling scheme for $\{(Me_2N)_3Zr[\mu\text{-}N(H)\ B_3(Me)_2N_3(Me)_3]\}_2$, 5.

composition and structure from **4**. A view of the molecule is shown in Fig. 7 and selected bond distances and bond angles are given in Table VI. The structure features a central, planar, asymmetric four-membered Zr_2N_2 ring in which each Zr atom is bonded to three terminal Me_2N groups and two bridging pentamethylborazinyl amido groups. The borazine rings planes are oriented perpendicular to the Zr_2N_2 plane with *cis* orientation across the plane. Two of the terminal Me_2N groups on each Zr atom are planar (N9, N11 on Zr1 and N12, N14 on Zr2) and these have significantly shorter Zr–N bond lengths, Zr1–N9 2.077(7) Å, Zr1–N11 2.062(7) Å, Zr2–N12 2.056(7) Å, Zr2–N14 2.057(8) Å, compared to the other two Me_2N groups that are pyramidal (sum of bond angles N10 333.1°, N13 333.7°) and display long Zr–N bond lengths, Zr1–N10 2.528(7) Å and Zr2–N13 2.530(8) Å. The Zr–N bond lengths in the central ring are Zr1–N1 2.043(7) Å, Zr1–N5 2.135(6) Å, Zr2–N1 2.131(7) and Zr2–N5 2.052(7) Å. It is interesting that these bridging amido groups have a planar heavy atom geometry with sums of bond angles N1, 359.2° and N5, 359.4°.

Compound **5** was obtained in analytically pure form, but a parent ion was not detected in the FAB-MS. NMR data, however, are fully consistent with the structure found in the solid state. The ^1H NMR spectrum contains singlets for the methyl groups on the boron atoms (B4,B6 δ 0.66), the N–H group (δ 1.39), the methyl groups on the ring nitrogen atoms (N5, δ 2.90, N1,N3, 3.21) and on the inequivalent Me_2N groups [δ 2,02, 2.05, 2.92) that appear in a 1:1:4 area ratio. Combinations of $Zr(NMe_2)_4$ with **3′** in hexane showed no evidence for reaction.

Based upon the model reactions of **3** and **3′**, it can be concluded that $Ti(NMe_2)_4$ and $Zr(NMe_2)_4$ should readily undergo transamination with terminal B–NH_2 groups in poly(borazinylamine) preceramic oligomer fragments such as idealized in **2**.

Table VI. Selected Bond Lengths (Å) and Bond Angles (°) for $\{(Me_2N)_3Zr[\mu\text{-}N(H)B_3(Me)_2N_3\ (Me)_3]\}_2$. **5**

Bond lengths			
Zr1–N1	2.043(7)	Zr1–N5	2.135(6)
Zr1–N9	2.077(7)	Zr1–N10	2.528(7)
Zr1–N11	2.062(7)	Zr2–N1	2.131(7)
Zr2–N5	2.052(7)	Zr2–N12	2.056(7)
Zr2–N13	2.530(8)	Zr2–N14	2.057(8)
Zr1•••Zr2	3.181(1)		
B1–N1	1.451(13)	B1–N2	1.447(12)
B1–N4	1.457(13)	B2–N2	1.432(15)
B2–N3	1.418(16)	B3–N3	1.423(14)
B3–N4	1.438(14)	B4–N5	1.440(14)
B4–N6	1.448(14)	B4–N8	1.456(13)
B5–N6	1.417(16)	B5–B7	1.447(18)
B6–N7	1.419(18)	B6–N8	1.431(17)
N2–C1	1.469(14)	B2–C2	1.578(16)
N3–C3	1.478(15)	B3–C4	1.578(16)
N4–C5	1.451(12)	B5–C7	1.591(19)
N6–C6	1.452(12)	B6–C9	1.596(17)
N7–C8	1.494(17)	N10–C13	1.466(15)
N8–C10	1.465(14)	N10–C14	1.471(12)
N9–C11	1.454(14)	N11–C15	1.435(13)
N9–C12	1.428(13)	N11–C16	1.460(14)
N12–C17	1.462(15)	N13–C19	1.474(13)
N12–C18	1.443(15)	N13–C20	1.459(13)
N14–C21	1.450(13)		
N14–C22	1.458(13)		
Bond angles			
N1–Zr1–N5	81.0(3)	N1–Zr1–N9	117.9(3)
N5–Zr1–N9	105.8(3)	N1–Zr1–N10	82.0(3)
N5–Zr1–N10	162.2(3)	N9–Zr1–N10	86.8(3)
N1–Zr1–N11	125.8(3)	N5–Zr1–N11	100.4(3)
N9–Zr1–N11	113.7(3)	N10–Zr1–N11	85.4(3)
N1–Zr2–N5	80.9(3)	N1–Zr2–N12	100.4(3)
N5–Zr2–N12	125.1(3)	N1–Zr2–N13	162.3(3)
N5–Zr2–N13	82.3(3)	N12–Zr2–N13	84.9(3)
N1–Zr2–N14	105.9(3)	N5–Zr2–N14	119.1(3)
Zr1–N1–Zr2	99.3(3)	Zr1–N5–Zr2	98.9(3)
Zr1–N1–B1	137.8(5)	Zr1–N5–B4	122.5(5)
Zr2–N1–B1	122.1(5)	Zr2–N5–B4	138.0(6)
N1–B1–N4	123.5(8)	N5–B4–N6	120.5(9)
N1–B1–N2	121.2(9)	N5–B4–N8	123.0(9)
N2–B1–N4	115.3(9)	N6–B4–N8	116.4(9)
C11–N9–C12	109.9(8)	C17–N12–C18	108.7(8)
Zr1–N9–C11	123.9(6)	Zr2–N12–C17	113.3(6)
Zr1–N9–C12	126.2(7)	Zr2–N12–C18	137.6(7)
C13–N10–C14	108.3(8)	C19–N13–C20	108.4(7)
Zr1–N10–C13	111.3(5)	Zr2–N13–C19	114.8(7)
Zr1–N10–C14	113.5(6)	Zr2–N13–C20	110.5(6)
C15–N11–C16	109.9(8)	C21–N14–C22	108.8(7)
Zr1–N11–C15	138.8(7)	Zr2–N14–C21	125.8(6)
Zr1–N11–C16	111.2(6)	Zr2–N14–C22	125.4(5)

Furthermore, it appears that there will be no or very little reactivity with the bridging B–N(H)–B groups. It also appears that the borazinylamine fragment has a much lower tendency toward cage aggregate formation compared to aniline and such aggregate formation would be further suppressed by the steric constraints imposed by the oligomer structure. The model chemistry, therefore, fully supports the concept of forming metallated poly(borazinylamine) oligomers that should be useful precursors for the formation of MN/BN ceramic composites.

3.2. Formation of Polymeric Precursors

Utilizing poly(borazinylamine) chemistry developed in our earlier work [7–19] we have examined the chemistry shown in Scheme 1. The 1:1 combination of 2-dimethylamino-4,6-dichloroborazine [7] with hexamethyldisilazane in hexane gives a white solid **11**. This material provides a CHN analysis comparable to samples prepared previously from chlorobenzene or hexane solution [7], and it is assumed to have the 2-point oligomer structure shown. Treatment of this solid with liquid NH_3 results in solvolysis of the terminal $–NMe_2$ groups and replacement with terminal $–NH_2$ groups. This is supported by CHN analytical data that show the retention of only a very small amount of carbon in **12**. Infrared spectra are also consistent with the replacement. The spectrum for **11** shows a relatively weak band at 3453 cm^{-1} that can be attributed to an N–H stretch for the bridging NH groups and bands at 2976, 2953, 2874 and 2874 cm^{-1} that can be tentatively assigned to NMe_2-methyl group stretching modes [7]. Following ammonolysis, the NMe_2 bands disappear and are replaced by medium to strong bands at 3486 and 3418 cm^{-1} that are assigned to the terminal $–NH_2$ vibrations. A weak band at 2955 cm^{-1} is present when the ammonolysis is incomplete, and this vibration is a sensitive indicator of the degree of completion of this chemistry.

Toluene slurries of oligomer **12** and $Ti(NMe_2)_4$ and $Zr(NMe_2)_4$ in an estimated 1:1 ratio, based upon one available $–NH_2$ group/borazine ring, were slurried at 23°C and then refluxed for 2 days. The exact composition and structure of the metallated oligomers are not known; however, some speculation is possible based upon IR data. For **13** (M = Ti), there is a medium intensity stretching frequency at 3422 cm^{-1} that can be tentatively assigned to a terminal N–H stretching vibration. This is downfrequency of the N–H stretch assigned to the oligomer υ_{NH2} band. The appearance of this band suggests that the transamination chemistry stops with the formation of an amido species $(Me_2N)_3Ti(NHR)$ (R = borazine ring fragment) and does not proceed on to an dimeric imido bridged species such as observed in the structure determined for **4**. In that regard, **4** does not display an IR band in the region 3500–3000 cm^{-1}. Both **13** and **4** show IR bands in the C–H stretch region 2950–2750 assigned to NCH_3 groups. Similarly for **15** (M = Zr), there is a medium intensity IR band at 3430 cm^{-1} that is assigned to an N–H stretch. This can be compared with the N–H

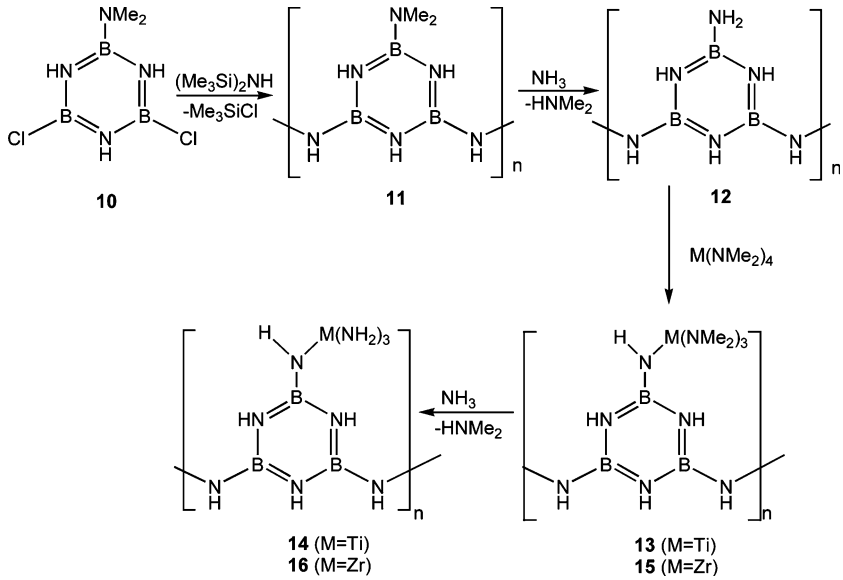

Scheme 1.

stretch at 3259 cm^{-1} observed in **5**. The higher value in **15** suggests that the species present may more resemble the monometallic product suggested in Scheme 1 than the dimeric bridging borazinylamine molecular product shown in Fig. 7.

The metallated oligomers **13** and **15** were then treated with liquid NH_3 for several hours in an effort to remove the terminal $-NMe_2$ groups on the metals replacing them with terminal $-NH_2$ or perhaps amino or imido bridge interactions formed subsequently *via* deamination. The objective was to reduce the level of carbon in the precursor oligomers **14** and **16** prior to pyrolysis. This treatment would also be expected to enhance the crosslinking in the oligomer and thereby reduce loss of material during pyrolysis. This is partially successful as bands attributed to C–H stretch modes in **14** and **16** are dramatically reduced in intensity following ammonolysis.

3.3. Pyrolysis of Preceramic Polymers

Thermogravimetric analyses (TGA) of **14** and **16** under argon were performed as a guide for the pyrolytic processing of the precursors. Oligomer **14** shows a gradual weight loss (~15 wt%) between 25° and 500°C and another 5% wt% loss between 600° and 800°C. The TGA for **16** is very similar except that a small weight loss (3–5 wt%) occurs between 900° and 1100°C. Using this information, bulk pyrolyses of samples of **14** and **16** were performed under a slow purge of NH_3 at 1200°C. A brown solid **17** (M = Ti) and a grey solid **18** (M = Zr) are obtained in ~70% yield. The elemental analysis for **17** is consistent with a formulation $Ti_{3.0}B_{5.4}N_{8.2}O_{1.0}C_{0.1}H_{0.3}$. The presence of ~4.8 wt% oxygen in the sample may result from partial hydrolysis of the oligomer **11** or **14** during sample handling prior to pyrolysis or from residual moisture in the flowing ammonia used for the pyrolysis reaction that takes place over a 6 h period. The low levels of carbon and hydrogen suggest that the ammonolysis of the preceramic polymer **11** with $NH_{3(l)}$ is effective. The powder XRD scan for **17** shows sharp reflections at d = 2.446, 2.117, 1.498, 1.277, and 1.222 that are in excellent agreement with d values for an authentic sample of c-TiN [49]. A weak, broad reflection with $d \cong 3.4$ corresponds to turbostratic BN. EDS analysis shows a prominent pair of peaks due to Ti. The SEM of the powder shows the formation of irregular shaped powder particles. On the other hand, TEM (Fig. 8) shows the distinct formation of cubic TiN particles, ~10 nm on a side, evenly distributed through a BN matrix. Selected area electron diffraction confirms the formation of nano-scale zones of crystalline TiN dispersed in h-BN matrix material.

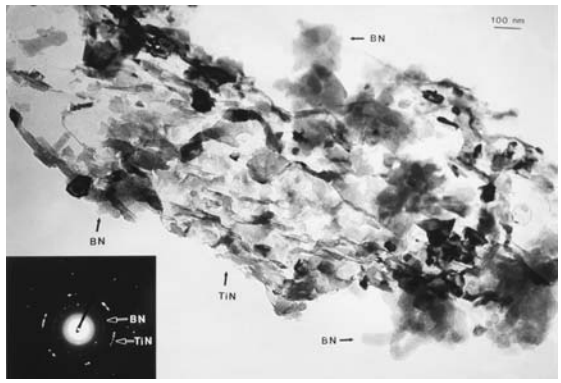

Fig. 8 Transmission electron micrograph for TiN/BN composite powder.(Space bar = 100 nm).

The elemental analysis of the grey powder **18** is consistent with the composition $Zr_{1.6}$ $B_{2.3}$ $N_{3.3}$ $O_{2.0}$ $H_{1.0}$ $C_{0.02}$. Once again, the oxygen impurity is relatively high (14 wt%) probably as a result of oligomer reactivity toward moisture. The infrared spectrum for the pyrolysis product shows strong absorptions due to boron nitride at 1377 cm^{-1} and 801 cm^{-1}. The powder X-ray diffraction pattern shows strong, sharp reflections at d = 2.631, 2.270, 1.614, 1.378 consistent with ZrN [50] and at d = 2.923, 2.541, 1.797, 1.533 ad 1.472 assigned to $ZrH_{0.6}N$ [51]. A low intensity broad hump also appears at $d \cong 3.4$ which corresponds to t-BN. The EDS for the powder shows three peaks for Zr. The SEM of the powder shows formation of irregular agglomerate particles. The TEM (Fig. 9), however, shows the formation of blocky nano-scale crystallites

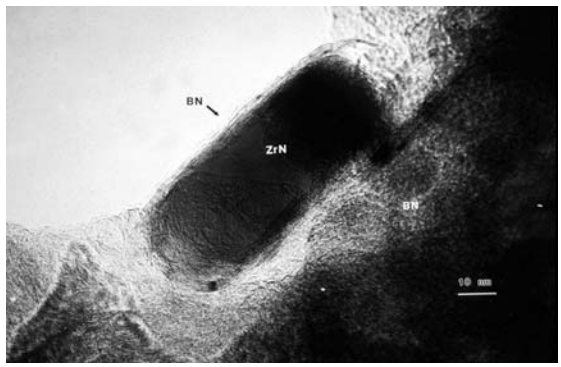

Fig. 9 Transmission electron micrograph for $ZrN/ZrH_{0.6}N/BN$ composite powder. (Space bar = 10 nm). Reprinted from Ref. [19], with permission from Elsevier.

of $ZrN/ZrH_{0.6}N$, ~5 nm on edge in a BN matrix. It is also noteworthy that the resolution of the TEM sample here shows the formation of an ordered hexagonal BN coating on the Zr nitride particles.

Seyferth and coworkers [52] and Sneddon and coworkers [53–55] have reported the use of preceramic polymers $[B_{10}H_{12}$·diamine$]_n$ and $(B_3N_3H_4)_n$, respectively, in combination with metals above 1000°C to form metal nitride/metal boride composites. In particular, Sneddon noted that polyborazylene completely reacts with Ti at 1000°C under argon with formation of TiN/TiB_2 and crystallization is complete at 1200°C [45–47]. A similar outcome was also found with Hf metal although the reaction was not complete until heated at 1450°C. We have not subjected our samples to temperatures above 1200°C; however, it appears at this temperature there is no evidence for the formation of crystalline borides. It should also be noted, as well, that the effective metal loadings in our systems are lower and we have employed a reactive ammonia pyrolysis atmosphere.

4. CONCLUSION

The results described above show that the primary amine, 1,3,4,5,6-pentamethyl-2-amino borazine, **3**, readily undergoes transamination with $Ti(NMe_2)_4$ and $Zr(NMe_2)_4$ forming molecular species distinct in composition and structure from those provided by the structurally similar aryl amine, aniline. Furthermore, the secondary amine bis(1,3,4,5,6-pentamethylborazinyl) amine, **3′**, does not appear to react with $Ti(NMe_2)_4$ and $Zr(NMe_2)_4$ under conditions that result in reactivity with diphenylamine. These differences in transamination reactivity between the borazinyl amines and aryl amines most likely reflect electronic factors that control nitrogen atom lone pair basicity and proton acidity for the respective amines. The observed reactivity of **3** and **3′** also support the utilization of a primary amine derivatized poly(borazinylamine) oligomer as a reagent for composite formation. We have described the formation of such an oligomer **12**. Transamination reaction chemistry between **12** and $Ti(NMe_2)_4$ and $Zr(NMe_2)_4$ results in metallated oligomers that upon pyrolysis produce TiN/BN and $ZrN/ZrH_{0.6}N$/B N composites in good yield. The composite powders have a uniform distribution of nano-scale metal nitride particles in a BN matrix and there is no evidence for the formation of metal borides under the conditions explored.

ACKNOWLEDGEMENT

Acknowledgement is made to the National Science Foundation (CHE-9983205) for financial support of this research.

REFERENCES

1. K. J. Wynne and R. W. Rice, *Ann. Rev. Mater. Sci.* **14**, 297 (1983).
2. C. K. Narula, *Ceramic Precursor Technology and Its Applications* (Marcell Dekker, NY, 1995).
3. B. Jaschke, U. Klingebiel, R. Riedel, N. Doslik, and R. Gadow, *Appl. Organometallic Chem.* **14**, 671 (2000).
4. M. Peuckert, T. Vaahs, and M. Bruck, *Adv. Mater.* **2**, 398 (1990).
5. J. Bill and F. Aldinger, *Adv. Mater.* **7**, 775 (1995).
6. P. Greil, *Adv. Engin. Mater.* **2**, 339 (2000).
7. C. K. Narula, R. Schaeffer, A. K. Datye, T. T. Borek, B. M. Rapko, and R. T. Paine, *Chem. Mater.* **2**, 384 (1990).
8. R. T. Paine and C. K. Narula, *Chem. Rev.* **90**, 73 (1990).
9. R. T. Paine and L. G. Sneddon, *ACS Symp. Ser.* **572**, 358 (1994).
10. R. T. Paine and L. G. Sneddon, *CHEMTECH*, July, 29 (1994).
11. C. K. Narula, R. Schaeffer, A. K. Datye, and R. T. Paine, *Inorg. Chem.* **28**, 4053 (1989).
12. C. K. Narula, D. A. Lindquist, M. Fan, T. T. Borek, E. N. Duesler, A. K. Datye, R. Schaeffer, and R. T. Paine, *Chem. Mater.* **2**, 377 (1990).
13. R. T. Paine, C. K. Narula, R. Schaeffer, and A. K. Datye, *Chem. Mater.* **1**, 486 (1989).
14. T. T. Borek, W. C. Ackerman, D. W. Hua, R. T. Paine, and D. M. Smith, *Langmuir* **7**, 2844 (1991).
15. J. F. Janik, W. C. Ackerman, R. T. Paine, D. W. Hua, A. Maskara, and D. M. Smith, *Langmuir* **10**, 514 (1994).
16. D. A. Lindquist, T. T. Kodas, D. M. Smith, X. Xiu, S. L. Hietala, and R. T. Paine, *J. Am. Ceram. Soc.* **74**, 3126 (1991).
17. D. A. Lindquist, J. F. Janik, A. K. Datye, and R. T. Paine, *Chem. Mater.* **4**, 17 (1992).
18. R. R. Rye, T. T. Borek, D. A. Lindquist, and R. T. Paine, *J. Am. Chem. Soc.* **73**, 1409 (1990).
19. R. T. Paine, J. F. Janik, and M. Fan, *Polyhedron* **13**, 1225 (1994).
20. D. C. Bradley and M. H. Chisholm, *Accts. Chem. Res.* **9**, 273 (1976).
21. M. F. Lappert, P. P. Power, A. R. Sanger, and R. C. Srivastava, *Metal and Metalloid Amides* (Ellis Norwood, Chischester, UK, 1980).
22. W. A. Nugent and B. L. Haymore, *Coord. Chem. Rev.* **31**, 123 (1980).
23. M. H. Chisholm and I. P. Rothwell, in *Comprehensive Coordination Chemistry*, G. Wilkinson, R. D. Gillard and J. A. McCleverty, eds.(Pergamon, Oxford, UK, 1987), pp. 161–188.
24. W. A. Nugent and J. M. Mayer, *Metal Ligand Multiple Bonds* (J. Wiley, NY, 1988).
25. D. E. Wigley, *Prog. Inorg. Chem.* **42**, 239 (1994).
26. D.C. Bradley and I. M. Thomas, *J. Chem. Soc.* 3857 (1960); ibid. *Proc. Chem. Soc.* 225 (1959).
27. M. H. Chisholm, C. E. Hammond, and J. C. Huffman, *Polyhedron* **7**, 2515 (1988).
28. D. L. Thorn, W. A. Nugent, and R. L. Harlow, *J. Am. Chem. Soc.* **103**, 357 (1981).
29. W. A. Nugent and R. L. Harlow, *Inorg. Chem.* **18**, 2030 (1979).
30. G. M. Brown and L. Maya, *J. Am. Ceram. Soc.* **71**, 78 (1988).

31. D. V. Baxter, M. H. Chisholm, G. J. Gama, and V. F. DiStasi, *Chem. Mater.* **8**, 1222 (1996).
32. R. Fix, R. G. Gordon, and D. M. Hoffman, *Chem. Mater.* **3**, 1138 (1991).
33. B. H. Weiller and B. V. Partido, *Chem. Mater.* **6**, 260 (1994).
34. J. B. Cross, S. M. Smith, and H. B. Schlegel, *Chem. Mater.* **13**, 1095 (2001).
35. L. H. Dubois, *Polyhedron* **13**, 1329 (1994).
36. J. N. Musher and R. G. Gordon, *J. Mater. Res.* **11**, 989 (1996).
37. B. H. Weiller, *J. Am. Chem. Soc.* **118**, 4975 (1996).
38. R. H. Toeniskoetter and F. R. Hall, *Inorg. Chem.* **2**, 29 (1963).
39. G. M. Sheldrick, *SHELXTL Operations Manual* (Nicolet XRD Corp, Cupertino, CA, 1981).
40. International Table for X-ray Crystallography, Vol. IV, (Kynock, Birmingham, UK, 1974).
41. D. C. Bradley and E. G. Torrible, *Can. J. Chem.* **41**, 134 (1963).
42. R. K. Bartlett, *J. Inorg. Nucl. Chem.* **28**, 2448 (1966).
43. M. Fan, E. N. Duesler, and R. T. Paine, *Applied Organomet. Chem.* **17**, 549 (2003).
44. M. E. Gross and T. Siegrist, *Inorg. Chem.* **31**, 4898 (1992).
45. S. Daniele, P. B. Hitchcock, M. F. Lappert, and P. G. Merle *J. Chem. Soc. Dalton Trans.* 3179 (2001).
46. S. Daniele, P. B. Hitchcock, M. F. Lappert, T. A. Nile, and Zdanski C. M. *J. Chem. Soc. Dalton Trans.* 3980 (2002).
47. M. E. Davie, T. Foerster, S. Parsons, C. Pulham, D. W. H. Rankin, and B. A. Smart, *Polyhedron* **25**, 923 (2006).
48. J. Fayos and D. Mootz, *Z. Anorg. Allgem. Chem.* **380**, 196 (1971).
49. JCPDS Index Card No. 38-1420, *Powder Diffraction File*, W. F. McClune, ed., JCPDS International Center for Diffraction Data; Swathmore PA.
50. JCPDS Index Card No. 31-1493, *Powder Diffraction File*, W. F. McClune, ed., JCPDS International Center for Diffraction Data; Swathmore PA.
51. JCPDS Indec Card No. 27-0996, *Powder Diffraction File*, W. F. McClune, ed., JCPDS International Center for Diffraction Data; Swathmore PA.
52. D. Seyferth, N. Bryson, D. P. Workman, and C. A. Sobon, *J. Am. Ceram. Soc.* **74**, 2687 (1991).
53. K. Su, M. Nowakowski, D. Bonnell, and L. G. Sneddon, *Chem. Mater.* **4**, 1139 (1992).
54. M. Nowakowski, K. Su, L. G. Sneddon, and D. Bonnell, *Mat. Res. Soc. Proc.* **286**, 425 (1993).
55. K. Forsthoefel and L. G. Sneddon, *J. Mater. Sci.* **39**, 6043 (2004).